

Technical feasibility of Magnetic Resonance Fingerprinting on a 1.5T MRI-Linac

T. Bruijnen^{1,2}, O. van der Heide², M.P.W. Intven¹, S. Mook¹,
J.J.W. Lagendijk¹, C.A.T. van den Berg^{1,2} and R.H.N.
Tijssen^{1,3}

¹ Department of Radiation Oncology, University Medical Center Utrecht, Utrecht, the Netherlands

² Computational Imaging Group for MRI diagnostics and therapy, Centre for Image Sciences, University Medical Center Utrecht, Utrecht, the Netherlands

³ Department of Radiation Oncology, Catharina Hospital, Eindhoven, the Netherlands

14 July 2020

Abstract. Hybrid MRI-linac (MRL) systems enable daily multiparametric quantitative MRI to assess tumor response to radiotherapy. Magnetic Resonance Fingerprinting (MRF) may provide time efficient means of rapid multiparametric quantitative MRI. The accuracy of MRF, however, relies on adequate control over system imperfections, such as eddy currents and B_1^+ , which are different and not as well established on MRL systems compared to diagnostic systems. In this study we investigate the technical feasibility of gradient spoiled 2D MRF on a 1.5T MRL. We show with phantom experiments that the MRL generates reliable MRF signals that are temporally stable during the day and have good agreement with spin-echo reference measurements. Subsequent *in-vivo* MRF scans in healthy volunteers and a patient with a colorectal liver metastasis showed good image quality, where the quantitative values of selected organs corresponded with the values reported in literature. Therefore we conclude that gradient spoiled 2D MRF is feasible on a 1.5T MRL with similar performance as on a diagnostic system. The precision and accuracy of the parametric maps are sufficient for further investigation of the clinical utility of MRF for online quantitatively MRI-guided radiotherapy.

Keywords: Radiotherapy, Magnetic Resonance Fingerprinting, MRI-Linac, Tumor response monitoring

Submitted to: *Phys. Med. Biol. as a technical note*

1. Introduction

One of the promises of magnetic resonance guided radiation therapy on hybrid MRI-linac (MRL) systems (Lagendijk *et al.* 2008, Mutic and Dempsey 2014, Fallone 2014, Keall *et al.* 2014) is the ability to assess tumor response on a daily basis. The daily response is currently assessed using anatomical imaging, but could be replaced with precise quantitative imaging techniques (van der Heide and Thorwarth 2018, Hall *et al.* 2019, Kooreman *et al.* 2019). Traditional quantitative imaging techniques based on steady-state methods, such as variable flip angle (T_1 -mapping) (Fram *et al.* 1987) or multi-echo spin echo (T_2 -mapping) (Meiboom and Gill 1958), however, require long acquisition times. The long scan times pose a considerable practical challenge as the on table time is almost entirely filled with anatomical imaging (i.e., high-resolution 3D anatomical imaging for daily plan adaptation and fast real-time imaging for tumor tracking). Typical MRL treatment fractions have at most a couple of minutes of free imaging time available such that it does not interfere with the clinical workflow (Raaymakers *et al.* 2017)(Fig.1-A). Therefore, the dual requirement of both fast and precise measurements mandates a sequence with a high precision per unit of time, i.e. quantification efficiency, for a practical implementation of online quantitative MRI-guided radiotherapy. Recently, transient-state-based quantitative imaging methods have been proposed to considerably improve this quantification efficiency. Magnetic resonance fingerprinting (MRF) (Ma *et al.* 2013, Jiang *et al.* 2015, Jiang *et al.* 2017) is such a transient-state method that enables rapid multiparametric imaging and therefore could be the ideal tool for therapy monitoring on the MRL.

Unlike steady-state methods, which aim to produce a constant MR signal over time, MRF deliberately creates a fluctuating signal (fingerprint) over the course of the acquisition, which is matched on a per voxel basis to a precomputed dictionary of signal responses during image reconstruction. The dictionary is populated with simulated responses for all possible tissue types, in terms of T_1 , T_2 and proton density, to the imposed transient-state MR sequence. Realistic simulations of these MR sequences are essential to accurately quantify the tissue properties (Ma *et al.* 2017, Assländer *et al.* 2017). Therefore, the simulation of the MR sequences requires adequate control over system imperfections such as eddy currents and heterogeneous magnetic fields (B_0 and B_1^+). These system imperfections are well characterised and controlled for diagnostic MR systems and MRF has been applied in multiple clinical studies (Badve *et al.* 2017, Rieger *et al.* 2018, Liao *et al.* 2018, Ma *et al.* 2019, Yu *et al.* 2017, Chen *et al.* 2016, Chen *et al.* 2019, Cavallo *et al.* 2019). However, these system imperfections are not yet accurately mapped in MRL systems. The 1.5T MRL system used in our institution (Unity, Elekta, Crawley, UK) differs from diagnostic systems in the split gradient and split magnet coil design, the radiolucent 2x4 channel receive coil and a paramagnetic rotating gantry that holds all the beam generating components (Fig.1-B). These hardware modifications have an impact on the system imperfections, such as reduced signal-to-

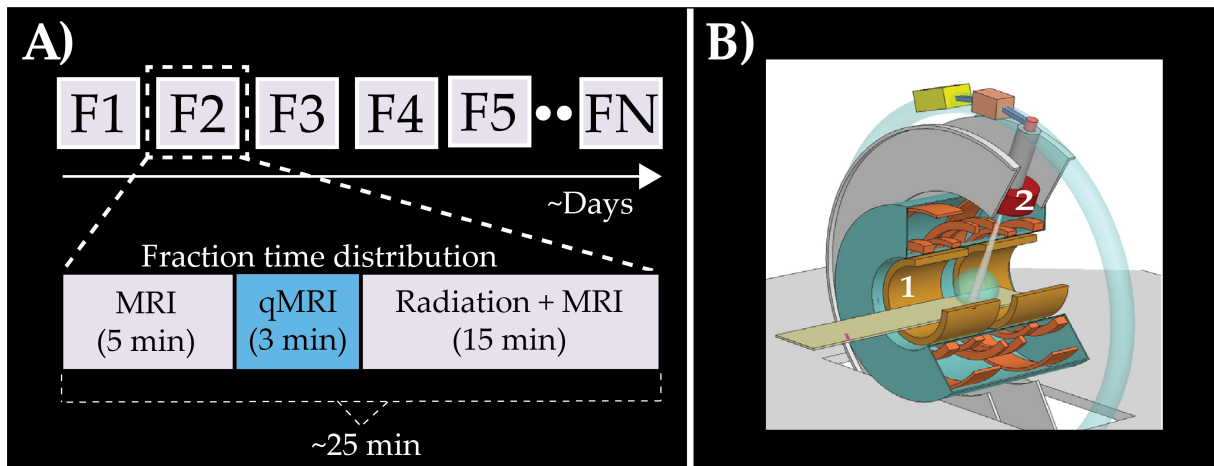


Figure 1. Schematic of a MRL radiotherapy treatment schedule. **A)** Example of a fractionation scheme where a patient is treated over multiple radiation fractions (F) distributed across multiple days. During each fraction, MR images are required for multiple purposes. During the first ≈ 5 minutes anatomical images are acquired for radiotherapy treatment planning. The treatment planning takes around 5 min (depending on plan complexity), which can be used for quantitative imaging. Finally the irradiation is started and requires continuous anatomical imaging for motion management. **B)** Impression of the MRL (Unity, Elekta) with the split gradient coil shown in yellow and the linear accelerator gun shown in red, as indicated with number 1 and 2 respectively.

noise ratio (Hoogcarspel *et al.* 2018, Zijlema *et al.* 2019), reduced uniformity of the static magnetic fields (B_1^+ and B_0) (Crijns and Raaymakers 2014, Jackson *et al.* 2019), reduced spatial region of gradient linearity (Tijssen *et al.* 2019) and different behavior of the eddy currents (Bruijnen *et al.* 2018). The impact of these system imperfections on the accuracy and precision of MRF parameter quantification is unknown. Therefore, an experimental study on the precision and accuracy of MRF is crucial for the potential application of daily quantitative tumor response monitoring on a 1.5T MRL.

In this work we investigate the technical feasibility of 2D MRF in phantoms and *in-vivo* on a 1.5T MRL. We assess the accuracy, precision and temporal stability of the parameter quantification in a phantom. In addition, we showcase typical image quality of the parameter maps in comparison with clinically used qualitative scans in volunteers and patients.

2. Materials and methods

2.1. MRF pulse sequence and reconstruction method

A 2D gradient spoiled MRF pulse sequence was implemented on a 1.5T Unity MR-linac equipped with a 2x4 channel radiation translucent receive array. Imaging data were acquired using the MRF sequence described by Jiang *et al.* (Jiang *et al.* 2015), which consists of an adiabatic inversion pulse and a sinusoidal flip angle train. One radial line was acquired per time-point (Cloos *et al.* 2016) and subsequent readouts were azimuthally incremented using the tiny golden angle to minimize eddy current effects (Wundrak *et al.* 2015, Bruijnen *et al.* 2019) (Fig.2). K-space data and k-space trajectory were corrected using the zeroth and first order gradient impulse response functions (Vannesjo *et al.* 2013, Bruijnen *et al.* 2018). Tissue fingerprints were simulated with extended phase graphs (Weigel 2015) with $T_1 \in [100 : 20 : 3000]$, $T_2 \in [20 : 10 : 1000]$ and inclusion of the slice profile (Ma *et al.* 2017). All data were used to estimate the coil sensitivities using ESPIRiT (Ong *et al.* 2015). MRF k-space data were reconstructed into singular value images with low rank inversion (Assländer *et al.* 2018) using the BART toolbox (Ong *et al.* 2015). The singular value images were subsequently matched with the dictionary to reconstruct the parametric maps. The code to perform the image reconstruction code and one MRF dataset are available on <https://github.com/tombrijnen/mrf-mrl>.

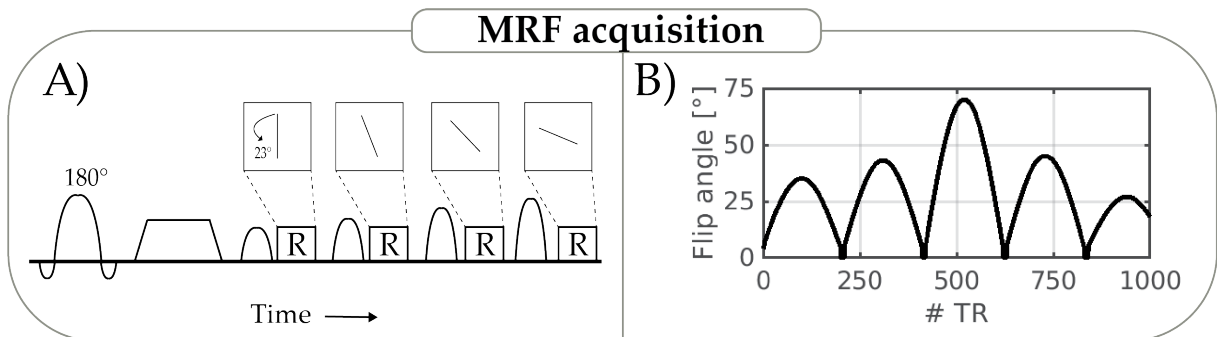


Figure 2. MRF acquisition overview. **A)** The MRF scan consists of an adiabatic inversion pulse followed 1000 radial readouts. The radial readouts are rotated with the tiny golden angle for each repetition time. **B)** The flip angle train used for all experiments. Note that the four flip angles shown in panel A) reflect the first four flip angles in the train.

2.2. Phantom studies

MRF data were acquired in a 2D transverse slice of 14 gadolinium-doped gel tubes (TO5, Eurospin II test system, Scotland). Relevant sequence parameters for all scans are shown in Table.1. One fully sampled dataset was acquired, which consists of 276 repeated measurements of the MRF flip angle train, where for each measurement the azimuthal

angle of the first spoke was rotated with the golden angle (111.2°). The measurements had a 10 second interval between repetitions to allow for full spin relaxation. Three and sixteen hours later MRF measurements were repeated with two minutes intervals for 30 minutes. Note that the fully sampled MRF scans were reconstructed with the maximum correlation method (Ma *et al.* 2013). In total these scans provide 306 MRF measurements, which are used to estimate the precision, temporal stability and accuracy of the parameter quantification. The precision was quantified by calculating the standard deviation of parameter values within a tube. The temporal stability was quantified by calculating the standard deviation of the mean value within the tube over the repeated measurements. The accuracy was quantified by calculating the mean value within a tube and comparing it to reference measurements. The reference measurements were acquired using two separate inversion recovery (T_1) and spin-echo (T_2) scans. The reference data were acquired with single echo spin-echo measurements with: voxel size = $3 \times 3 \times 10 \text{ mm}^3$ scan time = 60 min, repetition time = 10 s and 10 inversion times $\in [100:3000]$ ms or 10 echo times $\in [20:500]$ ms.

2.3. In-vivo studies

This study was approved by the institutional review board of the UMC Utrecht (Medisch Ethische Toetsingscommissie Utrecht (METC), ID:17-010, "MRI protocol development for MR-linac") and informed consent was obtained from all the participants. MRF data were acquired in the brain and upper abdomen of a healthy volunteer. One patient with a recurrent colorectal liver metastasis, after hepatic surgery, was scanned using the described MRF sequence with the addition of an custom developed abdominal compression corset to reduce motion artefacts (Heerkens *et al.* 2017). The complete MRI protocol consisted of multiple 2D MRF scans and qualitative T_1 and T_2 -w scans derived from the clinical protocol. The MRF scans in the upper abdomen were scanned in breathhold for the volunteer and in free-breathing for the patient. Regions of interest were manually selected on specific organs to compute the mean values, which were compared to literature values (de Bazelaire *et al.* 2004, Deoni *et al.* 2005). Relevant sequence parameters for all scans are shown in Table.1.

Table 1. Scanner and sequence parameters of the phantom and *in vivo* experiments.

MRF Sequence settings			
	Phantom	Brain	Abdomen
Field strength	1.5T	1.5T	1.5T
Spatial resolution	2.0 x 2.0 mm ²	1.5 x 1.5 mm ²	2.0 x 2.0 mm ²
Matrix size	125 x 125	186 x 186	175 x 175
Field-of-view	250 x 250 mm ²	280 x 280 mm ²	350 x 350 mm ²
Slick thickness	10 mm	5 mm	10 mm
Repetition time	5.2 ms	7.7 ms	5.3 ms
Echo time	2.5 ms	3.3 ms	2.5 ms
Readout bandwidth	386 Hz/pixel	285 Hz/pixel	379 Hz/pixel
N Flip angles	1000	1000	1000
Scan time	5.2 s	7.7 s	5.3 s

3. Results

3.1. Phantom studies

An exemplary time-point image of the fully sampled MRF scan along with the MRF proton density, T_1 and T_2 parameter maps are shown in Fig.3. The bottom row shows the raw time domain signal (fingerprint) of voxels in tube 1 and 11 along with the match to the dictionary. For both these voxels the time domain signal shows close agreement with the dictionary match. The agreement holds for all the pixels within the tubes with a mean normalized root mean square error (NRMSE) = 0.06. Small differences between the MRF signal and the dictionary match are primarily observed during the first 50 snapshots directly after the inversion pulse and during the higher flip angles in time-points 500-600.

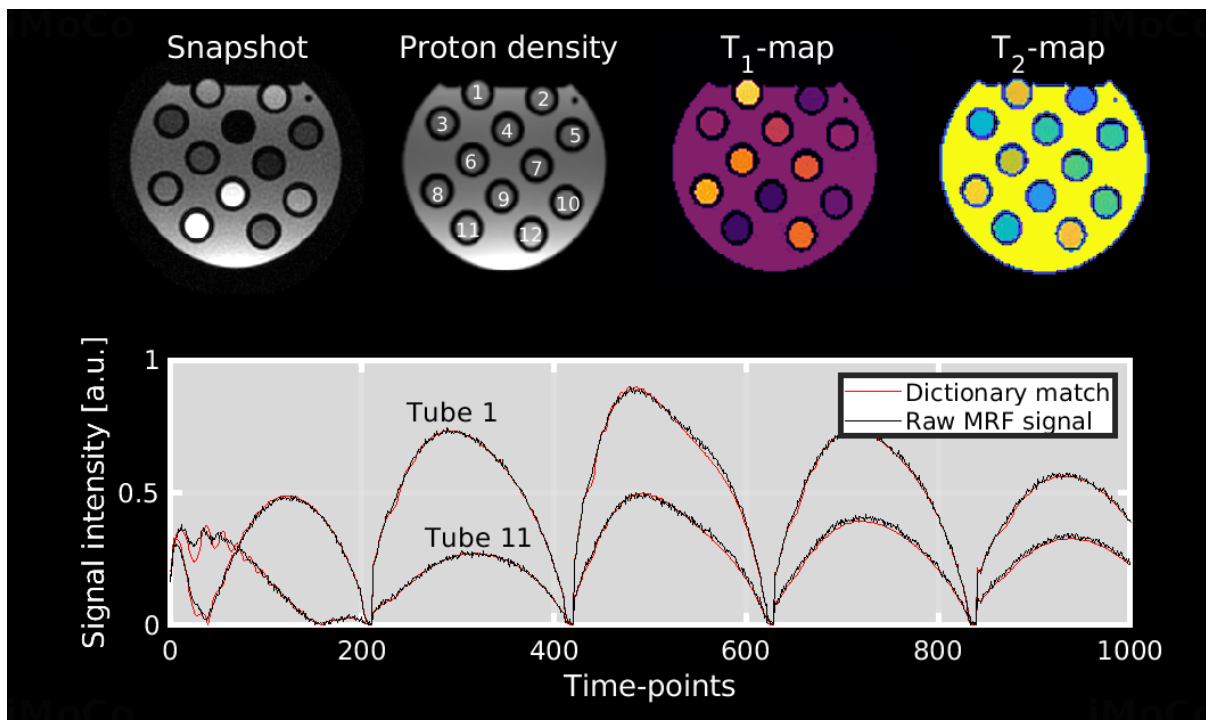


Figure 3. Analysis of the raw MRF time domain signal. Top row shows the images reconstructed from the fully sampled MRF measurements. From left-to-right a single time-point image(snapshot) and the reconstructed parameters maps. The bottom row shows the time domain signal of a voxel in tube 1 and a voxel in tube 11. Note that the time signals are in close agreement with the match to the dictionary. See the following link for an animated version: <https://surfdive.surf.nl/files/index.php/s/KavixXHVaq4c9Ue>

The parameter quantification of the fully sampled ($R=1$) and undersampled ($R=276$) MRF reconstructions are compared against the spin-echo reconstructions in Fig.4. Both the $R=1$ and $R=276$ MRF reconstructions showed good correlation in average values compared to the spin-echo measurements. The undersampled MRF has coefficients of determination $R_{T_1}^2 = 0.999$ and $R_{T_2}^2 = 0.975$ for T_1 and T_2 , respectively. Note that the accuracy of the T_1 -maps was slightly higher than the T_2 -maps. The precision over all the tubes for the undersampled MRF was $\sigma_{T_1} = 8.6$ ms and $\sigma_{T_2} = 3.0$ ms.

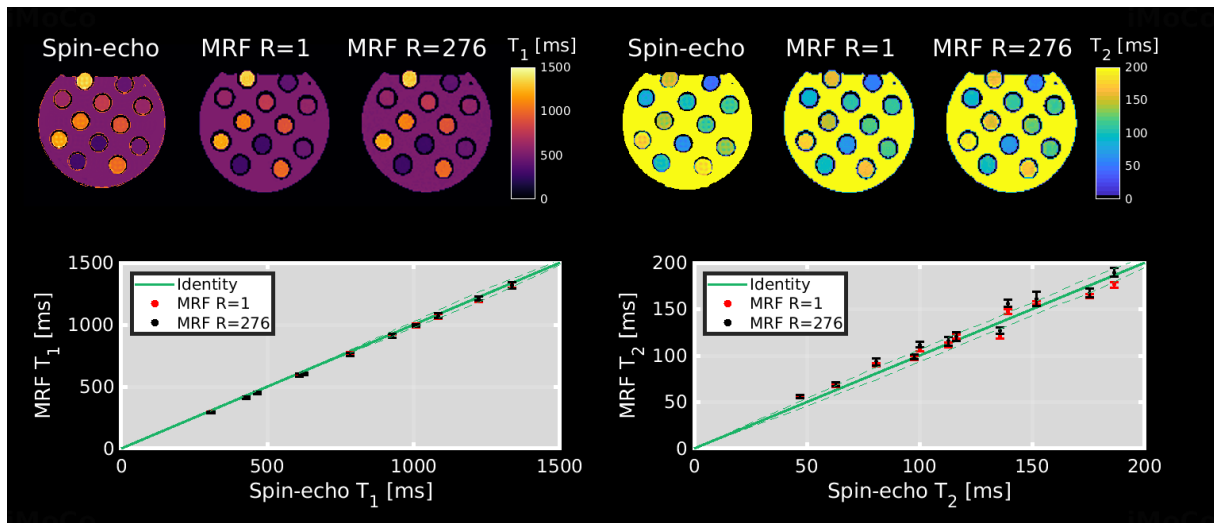


Figure 4. Accuracy and precision analysis of MRF parameter quantification in a phantom. Top row shows the spin-echo, fully sampled MRF and undersampled MRF parameter maps. The bottom row shows the correlation of the accuracy estimations for MRF versus the spin-echo. Data show the mean and standard deviation of MRF over a 25 pixel region in the center of the phantom. The dashed green line is the standard deviation of the spin-echo measurements in the same region.

The temporal stability of the parameter quantification (reproducibility) of the repeated measurements is shown in Fig.5. The T_1 values were very stable, while the higher T_2 values show slightly higher deviation over time. The mean values within the tubes had an average standard deviation over time of $\sigma_{T_1} = 6.4$ ms and $\sigma_{T_2} = 2.3$ ms.

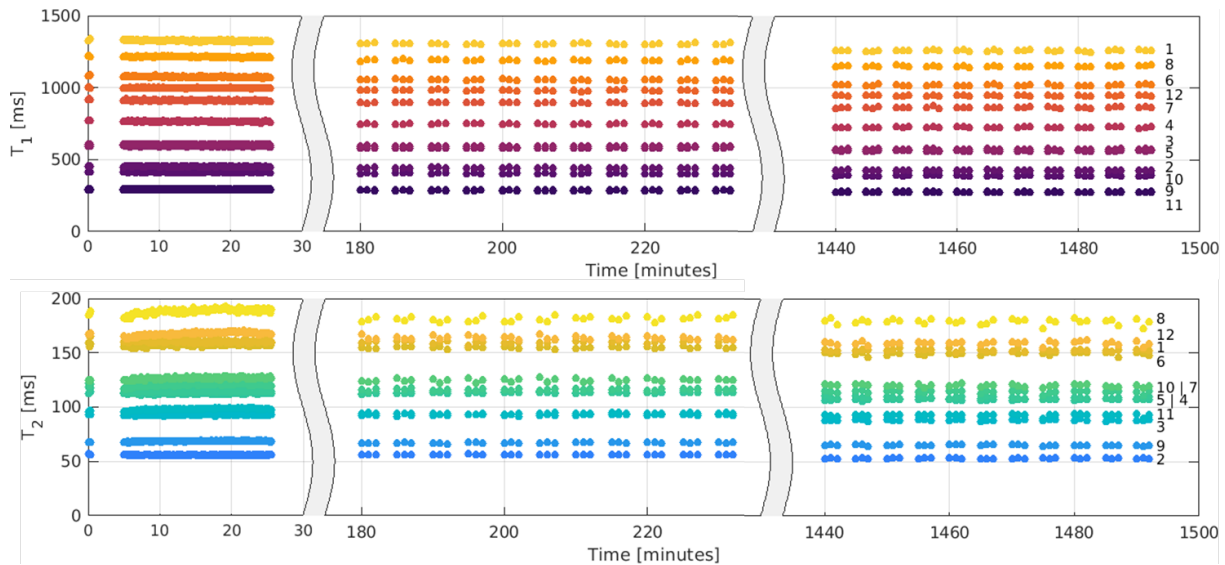


Figure 5. Repeated MRF measurement to assess the temporal stability of the parameter quantification. Top row shows the evolution of the mean T_1 values within the tubes and the bottom row shows the evolution of the T_2 values. Note that the tube numbers are added at the right side of the graph and they correspond with the numbers in Fig.3. See the following link for video that shows the parameter maps over time: <https://surfdribe.surf.nl/files/index.php/s/aOB3B2YlAxeT4mo>

3.2. In-vivo studies

Brain volunteer data

Two slices of the brain MRF scans in the volunteer are shown in Fig.6. The T_1 and T_2 maps show clear boundaries between white and gray matter. The mean parameter values for gray and white matter are within the range of report literature values (Table.2). Note that the T_2 values are on the low side, which is also reported in other MRF publications (Jiang *et al.* 2015). The regions of interest that were used to compute the mean values are shown on the proton density image.

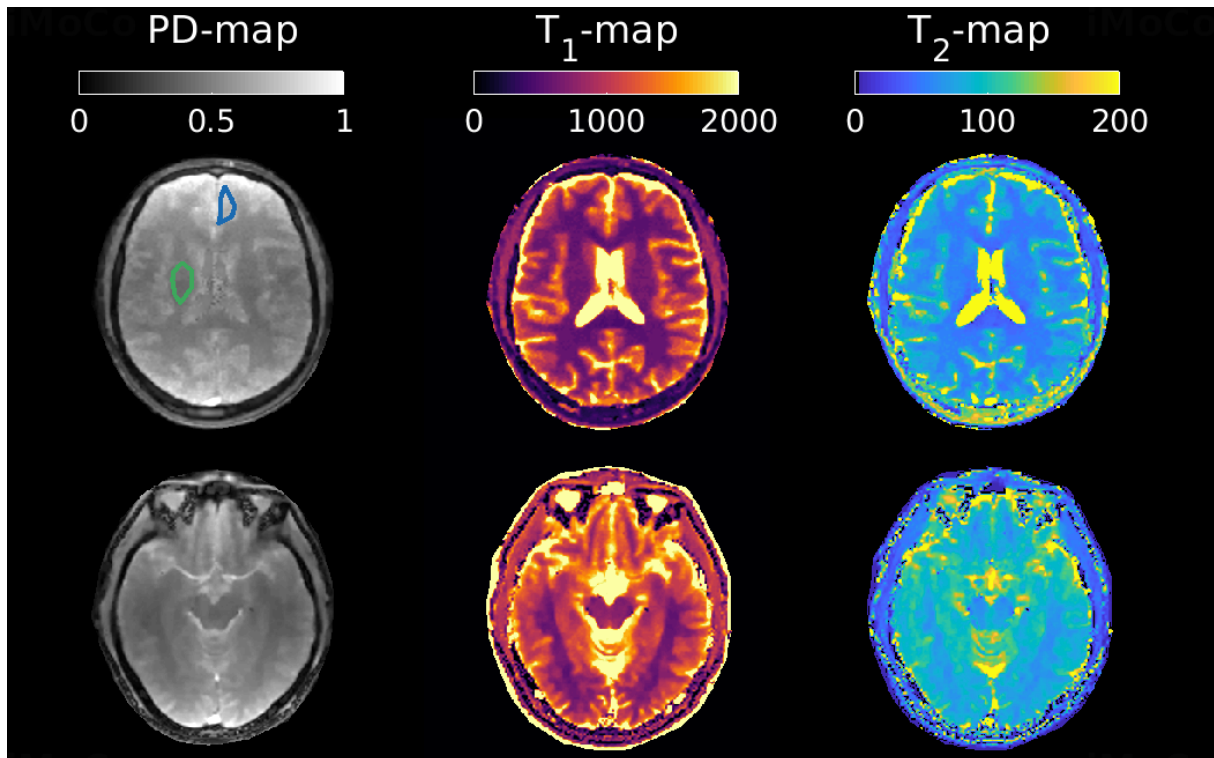


Figure 6. 2D brain MRF measurement in a healthy volunteer. Top row shows slice 1 of the MRF parameter maps and bottom row shows slice 2. Averaged $T_{1,2}$ values for white matter (green) and gray matter (blue) are shown in Table.2.

Table 2. Comparison of MRF T_1 and T_2 quantification to literature reported values. cite(de Bazelaire)

MRF parameter quantification				
	Reference T_1	MRF T_1	Reference T_2	MRF T_2
White matter	608 - 756 ms	626 ± 34 ms	54 - 81 ms	56 ± 4 ms
Gray matter	998 - 1304 ms	1113 ± 91 ms	78 - 98 ms	76 ± 7 ms
Liver	547 - 625 ms	612 ± 42 ms	40 - 52 ms	46 ± 5 ms
Kidney (medulla)	1354 - 1470 ms	1510 ± 144 ms	74 - 96 ms	51 ± 6 ms
Kidney (cortex)	908 - 1024 ms	954 ± 85 ms	83 - 91 ms	54 ± 5 ms
Pancreas	570 - 598 ms	540 ± 59 ms	40 - 52 ms	47 ± 8 ms

Volunteer abdomen data

Two slices of the abdomen MRF scans in the volunteer are shown in Fig.7-8. The boundaries between the medulla and cortex of the kidney are well defined on both the T_1 -map and the T_1 - w image, while the boundary is not visible on the T_2 - w image and T_2 -map. On the left side of the liver a small benign lesion is clearly visible on both the T_1 and T_2 map, which is characterised with a high T_1 and high T_2 . The T_2 values

differ between the right and left kidney, which are 35 and 51 ms respectively. Region of interest analysis for multiple organs are shown in Table.2. The kidney T_2 values also differ slightly between the two scans. However, the T_1 values were constant between the left and right kidney and between slice 1 and 2. The regions of interest that were used to compute the mean values are shown on the proton density image.

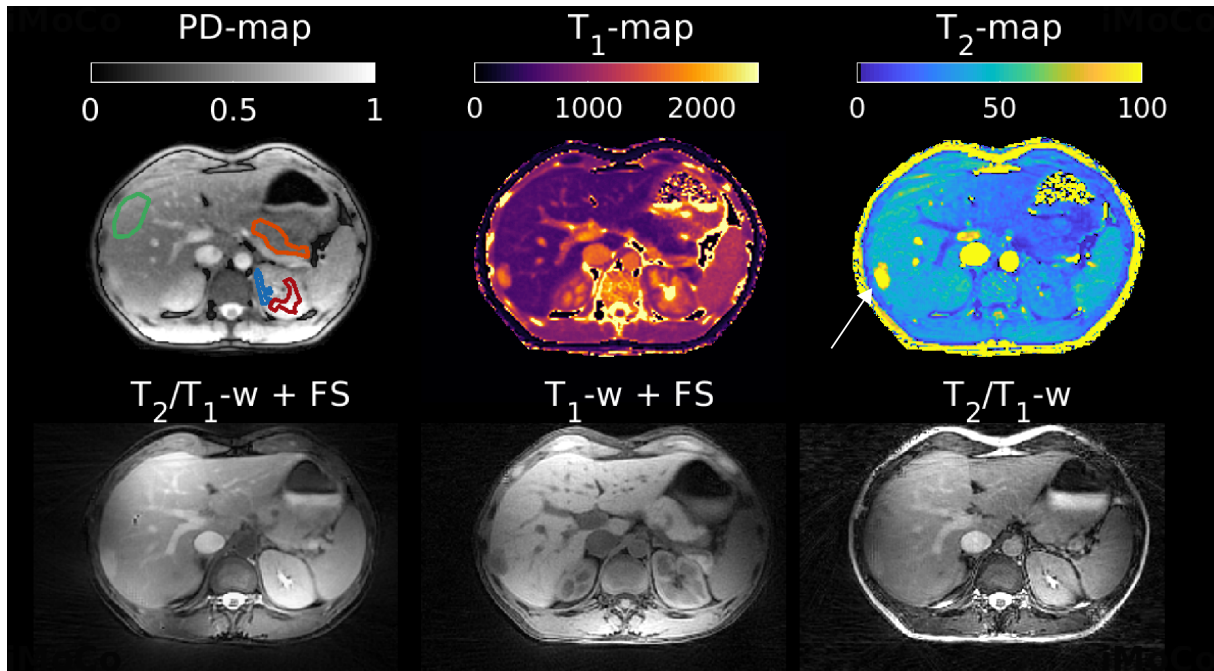


Figure 7. Breathhold 2D MRF measurement in a healthy volunteer. Top row shows the MRF parameter maps. Bottom row shows the qualitative images derived a clinical protocol. The T_1-w scan is a spoiled gradient echo sequence, the T_2/T_1-w is a balanced gradient echo scan and FS = fat suppression. Note that the lesion that is visible in the liver is a benign cyst indicated by the white arrow. Mean T_1 and T_2 values were analyzed in regions of interest for liver (green), pancreas (orange), medulla (red) and cortex (blue) of the kidney.

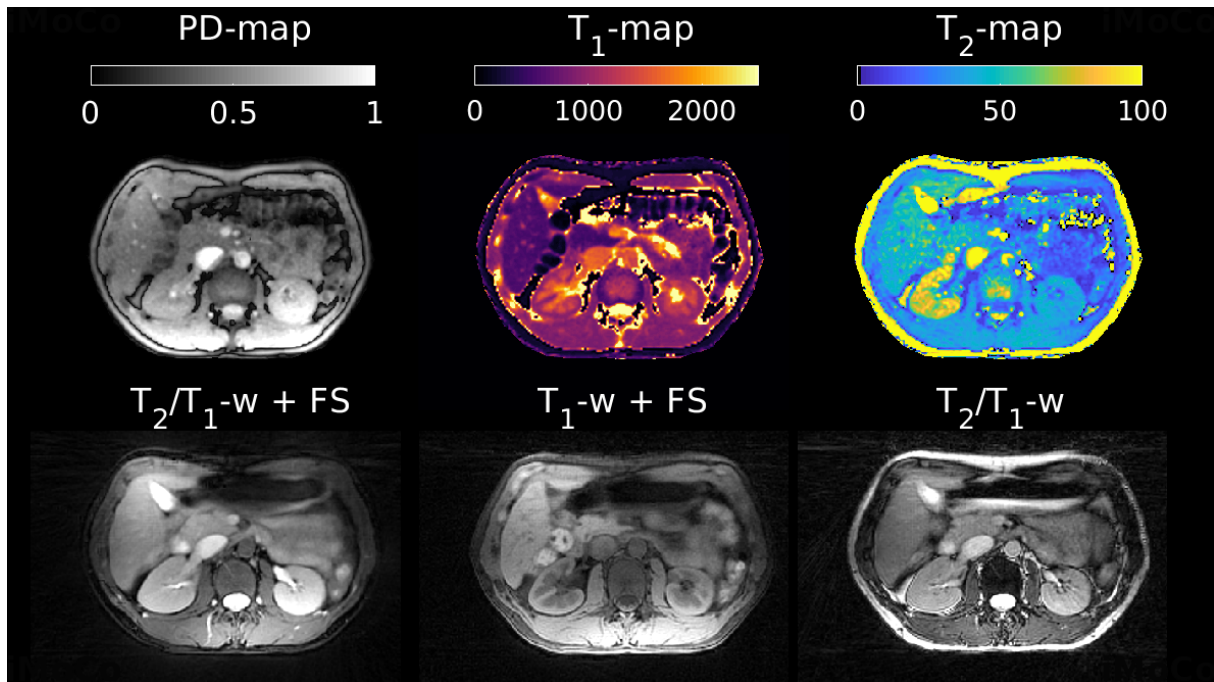


Figure 8. Breathhold 2D MRF measurement in a healthy volunteer. Top row shows the MRF parameter maps. Bottom row shows the qualitative images derived a clinical protocol. The T_1 -w scan is a spoiled gradient echo sequence, the T_2/T_1 -w is a balanced gradient echo scan and FS = fat suppression.

Patient abdomen data

One slice of the abdomen MRF scan in the patient with a recurrent colorectal liver metastasis after hepatic resection is shown in Fig.9. The metastasis is positioned in the anterior side of the liver and is clearly visible on the T_1 -map, T_1 -w image and on the diffusion-w image, while the lesion is less well defined on the T_2 -map and T_2 -w image. The T_2 -map shows lower values in the liver and spleen compared to the volunteer scans, which could be due to patient motion.

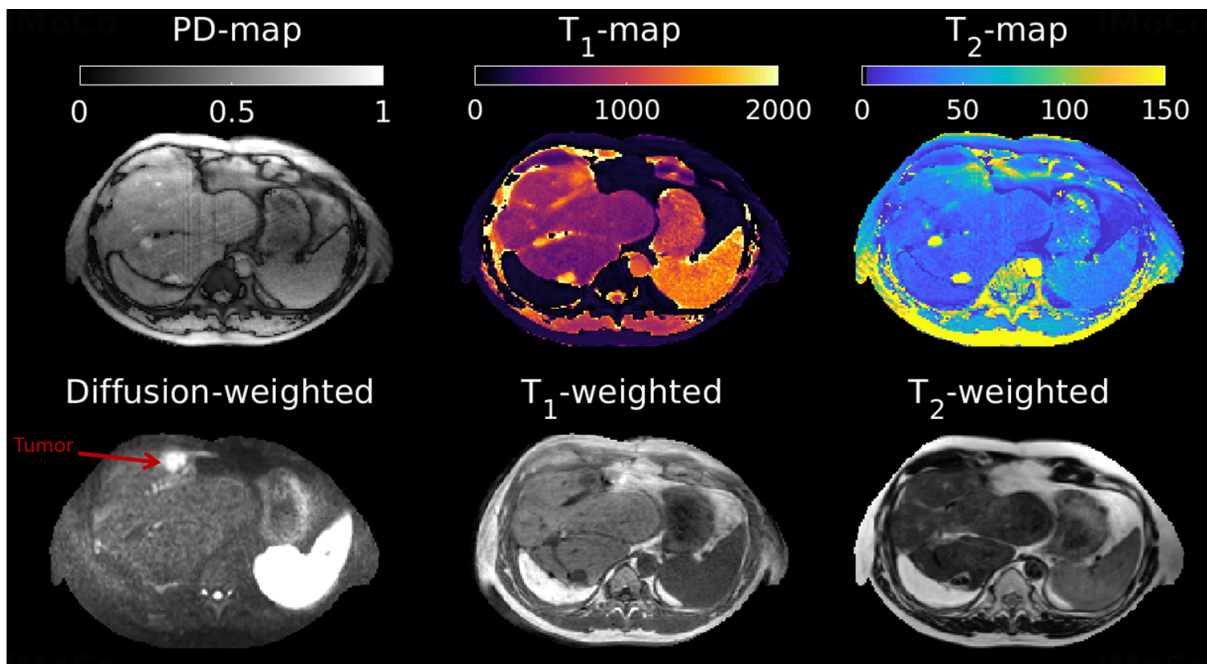


Figure 9. Free-breathing 2D MRF measurement in a patient with a colorectal liver metastasis. Top row shows the MRF parameter maps. Bottom row shows the qualitative images from the clinically used protocol. The T_1 - w scan is a spoiled gradient echo sequence, the T_2 - w is a turbo spin echo sequence and the diffusion- w is a spin-echo sequence with EPI readout. The lesion is indicated with the red arrow on the diffusion-weighted image and is also clearly visible on the T_1 scans.

4. Discussion

In this study we demonstrated technical feasibility of 2D MRF on a 1.5T MRL system. The phantom study indicated good agreement of parameter quantification ($R_{T_1}^2 = 0.999$ and $R_{T_2}^2 = 0.975$) with reference measurements, high precision ($\sigma_{T_1} = 8.6ms$ and $\sigma_{T_2} = 3.0ms$) and temporally stable measurements during the day ($\sigma_{T_1} = 6.4ms$ and $\sigma_{T_2} = 2.3ms$). The *in vivo* study showed high image quality of the fast MRF scans, where image features in the quantitative maps nicely corresponded with the qualitative scans. We believe these observations provide sufficient evidence that MRF is technically feasible on MRL systems and therefore could be further explored for online MR-guided radiotherapy applications on a 1.5T MRL. Besides MRF, these findings also apply for other transient-state parameter quantification methods (Sbrizzi *et al.* 2018).

A possible use case for the quantitative maps could be patient-specific contrast optimization of the anatomical turbo spin-echo sequences, i.e. the reference MRI on which the treatment is planned. For example, liver metastasis are a heterogeneous group of lesions that show variable signal characteristics on both T_1w and T_2w imaging depending on the primary origin (Danet *et al.* 2003, Namasivayam *et al.* 2007). In this context, MRF could function as a contrast scout scan followed by an on-the-fly flip angle train optimization to maximize the contrast-to-noise ratio between the lesion and the liver. Contrast optimization techniques are well described in literature (Sbrizzi *et al.* 2017), but have never been applied in an on-the-fly setting for online contrast optimization on either diagnostic MR systems or MRL systems. Future work will focus on the implementation of these patient-specific contrast optimization techniques to investigate the potential improvement in image quality.

The rapid acquisition scheme of MRF (≈ 5 s per slice) could facilitate the integration of quantitative imaging to the clinical MRI-guided radiotherapy workflow without significantly lengthening of the treatment. The primary application of MRF would be for tumor response monitoring over multiple fractions during the treatment. The optimal timing to image changes in quantitative parameters post radiotherapy is an active topic of research (Fang *et al.* 2018, van Schie *et al.* 2019, Borggreve *et al.* 2019) and could be pushed forward with daily MRF on the MRL. The ability to pick up subtle changes in T_1 and T_2 values could be used to distinguish responders from non-responders. Ultimately, these potential changes in T_1 and T_2 could be used to intensify or reduce the (local) radiation during the radiotherapy treatment period based on the measured response.

5. Conclusion

Gradient spoiled 2D magnetic resonance fingerprinting is feasible on a 1.5T MRI-Linac with similar performance as on a diagnostic system. The precision and accuracy of the

parametric maps are sufficient for further investigation of the clinical utility of magnetic resonance fingerprinting for online quantitatively MRI-guided radiotherapy.

Acknowledgements

This work is part of the research programme HTSM with project number 15354, which is (partly) financed by the Netherlands Organisation for Scientific Research (NWO) and Philips Healthcare.

References

- Assländer J, Cloos M A, Knoll F, Sodickson D K, Hennig J and Lattanzi R 2018 Low rank alternating direction method of multipliers reconstruction for MR fingerprinting *Magnetic Resonance in Medicine* **79**(1), 83–96.
- Assländer J, Glaser S J and Hennig J 2017 Pseudo Steady-State Free Precession for MR-Fingerprinting *Magnetic Resonance in Medicine* **77**(3), 1151–1161.
- Badve C, Yu A, Dastmalchian S, Rogers M, Ma D, Jiang Y, Margevicius S, Pahwa S, Lu Z, Schluchter M, Sunshine X J, Griswold M, Sloan A and Gulani V 2017 *in* ‘American Journal of Neuroradiology’ Vol. 38 American Society of Neuroradiology pp. 492–499.
- Borggreve A S, Heethuis S E, Boekhoff M R, Goense L, van Rossum P S, Brosens L A, van Lier A L, van Hillegersberg R, Lagendijk J J, Mook S, Ruurda J P and Meijer G J 2019 Optimal timing for prediction of pathologic complete response to neoadjuvant chemoradiotherapy with diffusion-weighted MRI in patients with esophageal cancer *European Radiology* pp. 1896–1907.
- Bruijnen T, Stemkens B, Lagendijk J J W, van den Berg C A T and Tijssen R H N 2018 Gradient system characterization of a 1.5T MRI-Linac with application to UTE imaging *International Society for Magnetic Resonance in Medicine (ISMRM)* p. 235.
- Bruijnen T, Stemkens B, van den Berg C A T and Tijssen R H N 2019 Prospective GIRF-based RF phase cycling to reduce eddy current-induced steady-state disruption in bSSFP imaging *Magnetic Resonance in Medicine* .
- Cavallo A U, Liu Y, Patterson A, Al-Kindi S, Hamilton J, Gilkeson R, Gulani V, Seiberlich N and Rajagopalan S 2019 ‘CMR Fingerprinting for Myocardial T1, T2, and ECV Quantification in Patients With Nonischemic Cardiomyopathy’.
- Chen Y, Jiang Y, Pahwa S, Ma D, Lu L, Twieg M D, Wright K L, Seiberlich N, Griswold M A and Gulani V 2016 MR Fingerprinting for Rapid Quantitative Abdominal Imaging *Radiology* .
- Chen Y, Panda A, Pahwa S, Hamilton J I, Dastmalchian S, McGivney D F, Ma D, Batesole J, Seiberlich N, Griswold M A, Plecha D and Gulani V 2019 Three-dimensional MR fingerprinting for quantitative breast imaging *Radiology* **290**(1), 33–40.
- Cloos M A, Knoll F, Zhao T, Block K T, Bruno M, Wiggins G C and Sodickson D K 2016 Multiparametric imaging with heterogeneous radiofrequency fields *Nature Communications* **7**.
- Crijns S and Raaymakers B 2014 From static to dynamic 1.5T MRI-linac prototype: Impact of gantry position related magnetic field variation on image fidelity *Physics in Medicine and Biology* **59**(13), 3241–3247.
- Danet I M, Semelka R C, Leonardou P, Braga L, Vaidean G, Woosley J T and Kanematsu M 2003 Spectrum of MRI appearances of untreated metastases of the liver *American Journal of Roentgenology* **181**(3), 809–817.
- de Bazelaire C M J, Duhamel G D, Rofsky N M and Alsop D C 2004 MR Imaging Relaxation Times of Abdominal and Pelvic Tissues Measured in Vivo at 3.0 T: Preliminary Results *Radiology* .
- Deoni S C, Peters T M and Rutt B K 2005 High-resolution T1 and T2 mapping of the brain in

- a clinically acceptable time with DESPOT1 and DESPOT2 *Magnetic Resonance in Medicine* **53**(1), 237–241.
- Fallone B G 2014 ‘The Rotating Biplanar Linac-Magnetic Resonance Imaging System’.
- Fang P, Musall B C, Son J B, Moreno A C, Hobbs B P, Carter B W, Fellman B M, Mawlawi O, Ma J and Lin S H 2018 Multimodal Imaging of Pathologic Response to Chemoradiation in Esophageal Cancer *International Journal of Radiation Oncology Biology Physics* **102**(4), 996–1001.
URL: <https://doi.org/10.1016/j.ijrobp.2018.02.029>
- Fram E K, Herfkens R J, Johnson G A, Glover G H, Karis J P, Shimakawa A, Perkins T G and Pelc N J 1987 Rapid calculation of T1 using variable flip angle gradient refocused imaging *Magnetic Resonance Imaging* **5**(3), 201–208.
- Hall W A, Paulson E S, van der Heide U A, Fuller C D, Raaymakers B W, Lagendijk J J, Li X A, Jaffray D A, Dawson L A, Erickson B, Verheij M, Harrington K J, Sahgal A, Lee P, Parikh P J, Bassetti M F, Robinson C G, Minsky B D, Choudhury A, Tersteeg R J and Schultz C J 2019 The transformation of radiation oncology using real-time magnetic resonance guidance: A review *European Journal of Cancer* **122**, 42–52.
URL: <https://doi.org/10.1016/j.ejca.2019.07.021>
- Heerkens H, Reerink O, Intven M, Hiensch R, van den Berg C, Crijns S, van Vulpen M and Meijer G 2017 Pancreatic tumor motion reduction by use of a custom abdominal corset *Physics and Imaging in Radiation Oncology* **2**, 7–10.
URL: <http://linkinghub.elsevier.com/retrieve/pii/S2405631616300173>
- Hoogcarspel S J, Zijlema S E, Tijssen R H, Kerkmeijer L G, Jürgenliemk-Schulz I M, Lagendijk J J and Raaymakers B W 2018 Characterization of the first RF coil dedicated to 1.5 T MR guided radiotherapy *Physics in Medicine and Biology* **63**(2).
- Jackson S, Glitzner M, Tijssen R H and Raaymakers B W 2019 MRI B 0 homogeneity and geometric distortion with continuous linac gantry rotation on an Elekta Unity MR-linac *Physics in Medicine and Biology* **64**(12).
- Jiang Y, Ma D, Keenan K E, Stupic K F, Gulani V and Griswold M A 2017 Repeatability of magnetic resonance fingerprinting T1 and T2 estimates assessed using the ISMRM/NIST MRI system phantom *Magnetic Resonance in Medicine* **78**(4), 1452–1457.
- Jiang Y, Ma D, Seiberlich N, Gulani V and Griswold M A 2015 MR fingerprinting using fast imaging with steady state precession (FISP) with spiral readout *Magnetic Resonance in Medicine* **74**(6), 1621–1631.
- Keall P J, Barton M and Crozier S 2014 The Australian Magnetic Resonance Imaging-Linac Program *Seminars in Radiation Oncology* **24**(3), 203–206.
URL: <http://dx.doi.org/10.1016/j.semradonc.2014.02.015>
- Kooreman E S, van Houdt P J, Nowee M E, van Pelt V W, Tijssen R H, Paulson E S, Gurney-Champion O J, Wang J, Koetsveld F, van Buuren L D, ter Beek L C and van der Heide U A 2019 Feasibility and accuracy of quantitative imaging on a 1.5 T MR-linear accelerator *Radiotherapy and Oncology* **133**, 156–162.
- Lagendijk J J W, Raaymakers B W, Raaijmakers A J E, Overweg J, Brown K J, Kerkhof E M, van der Put R W, Hårdemark B, van Vulpen M and van der Heide U A 2008 MRI/linac integration *Radiotherapy and Oncology* **86**(1), 25–29.
- Liao C, Wang K, Cao X, Li Y, Wu D, Ye H, Ding Q, He H and Zhong J 2018 Detection of lesions in mesial temporal lobe epilepsy by using MR fingerprinting *Radiology* **288**(3), 804–812.
- Ma D, Coppo S, Chen Y, McGivney D F, Jiang Y, Pahwa S, Gulani V and Griswold M A 2017 Slice profile and B1 corrections in 2D magnetic resonance fingerprinting *Magnetic Resonance in Medicine* .
- Ma D, Gulani V, Seiberlich N, Liu K, Sunshine J L, Duerk J L and Griswold M A 2013 Magnetic resonance fingerprinting *Nature* .
- Ma D, Jones S E, Deshmone A, Sakaie K, Pierre E Y, Larvie M, McGivney D, Blümcke I, Krishnan B, Lowe M, Gulani V, Najm I, Griswold M A and Wang Z I 2019 Development of high-resolution

- 3D MR fingerprinting for detection and characterization of epileptic lesions *Journal of Magnetic Resonance Imaging* **49**(5), 1333–1346.
- Meiboom S and Gill D 1958 Modified spin-echo method for measuring nuclear relaxation times *Review of Scientific Instruments* **29**(8), 688–691.
- Mutic S and Dempsey J F 2014 ‘The ViewRay System: Magnetic Resonance-Guided and Controlled Radiotherapy’.
- Namasivayam S, Martin D R and Saini S 2007 Imaging of liver metastases: MRI *Cancer Imaging* **7**(1), 2–9.
- Ong F, Uecker M, Tariq U, Hsiao A, Alley M T, Vasanaawala S S and Lustig M 2015 Berkeley Advanced Reconstruction Tools *Proc. Intl. Soc. Mag. Reson. Med.* **73**(2), 828–842.
URL: <https://lists.eecs.berkeley.edu/sympa/info/mrirecon>
- Raaymakers B W, Jürgenliemk-Schulz I M, Bol G H, Glitzner M, Kotte A N, Van Asselen B, De Boer J C, Bluemink J J, Hackett S L, Moerland M A, Woodings S J, Wolthaus J W, Van Zijp H M, Philippens M E, Tijssen R, Kok J G, De Groot-Van Breugel E N, Kiekebosch I, Meijers L T, Nomden C N, Sikkes G G, Doornaert P A, Eppinga W S, Kasperts N, Kerkmeijer L G, Tersteeg J H, Brown K J, Pais B, Woodhead P and Lagendijk J J 2017 First patients treated with a 1.5 T MRI-Linac: Clinical proof of concept of a high-precision, high-field MRI guided radiotherapy treatment *Physics in Medicine and Biology* **62**(23), L41–L50.
URL: <http://iopscience.iop.org/article/10.1088/1361-6560/aa9517/pdf>
- Rieger B, Akçakaya M, Pariente J C, Llufrui S, Martinez-Heras E, Weingärtner S and Schad L R 2018 Time efficient whole-brain coverage with MR Fingerprinting using slice-interleaved echo-planar-imaging *Scientific Reports* **8**(1).
- Sbrizzi A, Hoogduin H, Hajnal J V, van den Berg C A, Luijten P R and Malik S J 2017 Optimal control design of turbo spin-echo sequences with applications to parallel-transmit systems *Magnetic Resonance in Medicine* **77**(1), 361–373.
- Sbrizzi A, van der Heide O, Cloos M, van der Toorn A, Hoogduin H, Luijten P R and van den Berg C A T 2018 Fast quantitative MRI as a nonlinear tomography problem *Magnetic Resonance Imaging* pp. 56–63.
- Tijssen R H, Philippens M E, Paulson E S, Glitzner M, Chugh B, Wetscherek A, Dubec M, Wang J and van der Heide U A 2019 MRI commissioning of 1.5T MR-linac systems a multi-institutional study *Radiotherapy and Oncology* **132**, 114–120.
- van der Heide U A and Thorwarth D 2018 Quantitative Imaging for Radiation Oncology *International Journal of Radiation Oncology Biology Physics* **102**(4), 683–686.
- van Schie M A, van Houdt P J, Ghobadi G, Pos F J, Walraven I, de Boer H C, van den Berg C A, Smeenk R J, Kerkmeijer L G and van der Heide U A 2019 Quantitative MRI Changes During Weekly Ultra-Hypofractionated Prostate Cancer Radiotherapy With Integrated Boost *Frontiers in Oncology* **9**(December).
- Vannesjo S J, Haerberlin M, Kasper L, Pavan M, Wilm B J, Barmet C and Pruessmann K P 2013 Gradient system characterization by impulse response measurements with a dynamic field camera *Magnetic Resonance in Medicine* .
- Weigel M 2015 ‘Extended phase graphs: Dephasing, RF pulses, and echoes - Pure and simple’.
- Wundrak S, Paul J, Ulrici J, Hell E and Rasche V 2015 A small surrogate for the golden angle in time-resolved radial MRI based on generalized fibonacci sequences *IEEE Transactions on Medical Imaging* **34**(6), 1262–1269.
- Yu A C, Badve C, Ponsky L E, Pahwa S, Dastmalchian S, Rogers M, Jiang Y, Margevicius S, Schluchter M, Tabayoyong W, Abouassaly R, McGivney D, Griswold M A and Gulani V 2017 Development of a combined Mr Fingerprinting and Diffusion examination for Prostate cancer *Radiology* **283**(3), 729–738.
- Zijlema S E, Tijssen R H, Malkov V N, Van Dijk L, Hackett S L, Kok J G, Lagendijk J J and Van Den Berg C A 2019 Design and feasibility of a flexible, on-body, high impedance coil receive array for a 1.5 T MR-linac *Physics in Medicine and Biology* **64**(18).